Seismic structure in central Mexico: Implications for fragmentation of the subducted Cocos plate

Sara L. Dougherty,[1] Robert W. Clayton,[1] and Don V. Helmberger[1]

Received 14 June 2012; revised 21 August 2012; accepted 22 August 2012; published 29 September 2012.

[1] The fine-scale seismic structure of the central Mexico subduction zone is studied using moderate-sized (M4-6) intraslab earthquakes. Regional waveforms from the Mapping the Rivera Subduction Zone (MARS) seismic array are complicated and contain detailed information about the subduction zone structure, including evidence of lateral heterogeneity. This waveform information is used to model the structure of the subducted plates, particularly along the transition from flat to normal subduction, where recent studies have shown evidence for possible slab tearing along the eastern projection of the Orozco Fracture Zone (OFZ). The lateral extent of a thin ultra-slow velocity layer (USL) imaged atop the Cocos slab in recent studies along the Meso America Subduction Experiment array is examined here using MARS waveforms. We find an edge to this USL which is coincident with the western boundary of the projected OFZ region. Forward modeling of the 2D structure of the subducted Rivera and Cocos plates using a finite difference algorithm provides constraints on the velocity and geometry of each slab's seismic structure in this region and confirms the location of the USL edge. We propose that the Cocos slab is currently fragmenting into a North Cocos plate and a South Cocos plate along the projection of the OFZ, in agreement with observations of variable Cocos plate motion on either side of the OFZ. This tearing event may be a young analogy to the 10 Ma Rivera-Cocos plate boundary, and may be related to the slab rollback in central Mexico.

Citation: Dougherty, S. L., R. W. Clayton, and D. V. Helmberger (2012), Seismic structure in central Mexico: Implications for fragmentation of the subducted Cocos plate, *J. Geophys. Res.*, *117*, B09316, doi:10.1029/2012JB009528.

1. Introduction

[2] The tectonic evolution of the northeast Pacific has been characterized by the fragmentation of lithospheric plates as segments of spreading centers approached the trench off the west coast of North America. During the last 55 million years, the Farallon plate and its remnants have been fragmenting into progressively smaller plates as the Pacific-Farallon ridge approached the subduction zone, with each new plate moving independently and becoming less stable through time [*Wortel and Cloetingh*, 1981, 1983; *Atwater*, 1989; *Lonsdale*, 1991; *Stock and Lee*, 1994]. These fragmentation events generally occurred along a fracture zone that represented a line of weakness between areas of the plate experiencing driving forces of differing magnitude or direction [*Lonsdale*, 1991]. The most recent of these fragmentation events occurred when the Rivera plate separated from the proto-Cocos plate about 10 Ma [*Klitgord and Mammerickx*, 1982; *DeMets and Traylen*, 2000].

[3] The Rivera and Cocos plates are subducting beneath the North American plate along the Middle American Trench (MAT) in central Mexico with convergence rates increasing from 1.1 cm/yr at 106.5°W to 2.4 cm/yr at 105°W and from 4.8 cm/yr at 104.5°W to 7.5 cm/yr at 94°W, respectively [*DeMets et al.*, 1990]. The age of the oceanic crust being subducted at the MAT also increases from about 10 Ma in the west to about 23 Ma in the east [*Pardo and Suárez*, 1995]. These young oceanic plates exhibit large lateral variations in slab dip, with a shallow subhorizontal segment bounded by segments that dip much more steeply [*Pardo and Suárez*, 1995]. Receiver functions and seismic velocity tomography along the Meso America Subduction Experiment (MASE) array show that the Cocos slab is horizontal for about 250 km beneath the North American plate in the Guerrero region, before steeply subducting with a dip of 75° at the southern margin of the Trans Mexican Volcanic Belt (TMVB) and truncating at a depth of 500 km [*Pérez-Campos et al.*, 2008; *Husker and Davis*, 2009; *Kim et al.*, 2010]. To the north and south, the dip angle of the Cocos slab increases gradually from 0° to ~50° and ~30°, respectively, whereas the Rivera plate subducts at a dip of about 50° [*Pardo and Suárez*, 1995].

[1]Seismological Laboratory, California Institute of Technology, Pasadena, California, USA.

Corresponding author: S. L. Dougherty, Seismological Laboratory, California Institute of Technology, MC 252-21, Pasadena, CA 91125, USA. (sarad@gps.caltech.edu)

0148-0227/12/2012JB009528

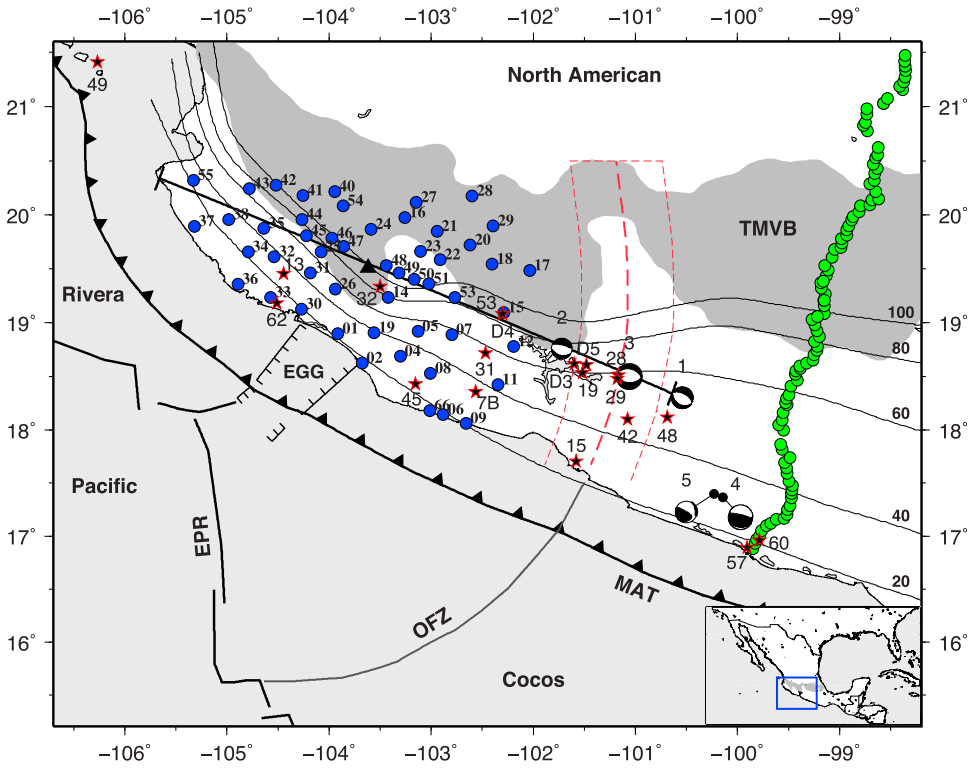

Figure 1. Map showing the MARS stations (blue dots) and events (stars, focal mechanisms) used in this study. Locations of MASE (green dots) stations are also shown for reference. The dark grey shaded area indicates the Trans Mexican Volcanic Belt (TMVB), and the black triangle denotes Colima Volcano. Slab isodepth contours from *Pardo and Suárez* [1995] are shown in thin lines. The projected path of the Orozco Fracture Zone (OFZ) beneath the North American plate is shown as a thick, red dashed line, with thinner, red dashed lines to either side delineating the estimated 100 km width of the fracture zone [*Blatter and Hammersley*, 2010]. The thick northwest-southeast trending line marks the location of the data profile and 2D velocity model cross-section. Other abbreviations shown in the map are EPR, East Pacific Rise; MAT, Middle America Trench; EGG, El Gordo Graben.

[4] Although the location and nature of the Rivera-Cocos plate boundary has long been contested [e.g., *Nixon*, 1982; *Eissler and McNally*, 1984; *Bourgois and Michaud*, 1991; *DeMets and Wilson*, 1997], recent studies have shown that it lies beneath the Colima Graben on land and its offshore extension to the southwest, the El Gordo Graben [e.g., *Stock and Lee*, 1994; *Bandy et al.*, 1995, 2000; *Serrato-Díaz et al.*, 2004]. These prominent extensional structures likely formed in response to divergence between the subducting Rivera and Cocos plates [*Ferrari et al.*, 1994; *Bandy et al.*, 1995, 1998, 2000; *Serrato-Díaz et al.*, 2004]. Seismic tomography imaging using data from the Mapping the Rivera Subduction Zone (MARS) array shows a clear gap between the Rivera and Cocos slabs starting at a depth of about 150 km and increasing with depth [*Yang et al.*, 2009]. This tear between the plates occurs beneath the Colima Graben and is suggested to be responsible for the location of Colima volcano and the graben itself [*Soto et al.*, 2009; *Yang et al.*, 2009].

[5] Further fragmentation of the Cocos plate has been proposed to be actively occurring along the Orozco Fracture Zone (OFZ) based on variations in plate motions observed on either side of the OFZ [*DeMets et al.*, 1990; *DeMets and Wilson*, 1997; *Bandy et al.*, 2000], the approach of the Pacific-Cocos spreading center toward the MAT [*Bandy and Hilde*, 2000], and the presence of a possible rift-rift-rift triple junction overlying the landward projection of the OFZ [*Bandy et al.*, 2000]. This ongoing fragmentation event may be occurring by a process analogous to that which occurred when the Rivera plate separated from the proto-Cocos plate. The tearing of the plate may provide a short-cut mechanism related to the trench-parallel flow associated with the rollback of the slab in central Mexico [*Russo and Silver*, 1994; *Ferrari*, 2004]. In order to test this hypothesis, we use regional earthquakes recorded by the MARS array to study the fine-scale structure of the central Mexico subduction zone along the transition from flat to normal subduction, where the eastern projection of the OFZ lies (Figure 1) [*Blatter and Hammersley*, 2010]. We perform 1D and 2D waveform modeling to image the structure of the slab and overriding plate. We also use observed waveform complexities to map the lateral extent of a thin ultra-slow velocity layer (USL) that was imaged atop the flat Cocos slab by the MASE array [*Pérez-Campos et al.*, 2008; *Song et al.*, 2009; *Kim et al.*, 2010] to test if the USL ends along a lineament related to the landward projection of the OFZ.

2. Data Analysis

2.1. Data

[6] The seismic data used in this study were provided by the MARS array, which consisted of 50 broadband seismic

Table 1. Events Used in This Study and Their Source Parameters

Event ID	Date	Latitude (deg)	Longitude (deg)	Depth (km)	Magnitude	Mechanism Strike/Dip/Rake	Source[a]
1	2006/02/20	18.30	−100.54	56	5.2	297/57/-93	1
2	2006/03/20	18.76	−101.72	64	4.9	282/59/-91	1
3	2006/08/11	18.50	−101.06	68	6.2	281/41/-83	2
4	2007/04/13	17.37	−100.14	43	6.0	284/73/92	1
5	2007/04/13	17.40	−100.23	67	5.3	297/90/119	1
7B	2006/02/17	18.35	−102.56	44	4.3	—	3
13	2006/03/30	19.46	−104.44	85	4.2	—	4
15	2006/05/16	17.71	−101.58	43	4.1	—	4
19	2006/06/07	18.54	−101.52	63	4.2	—	4
28	2006/08/11	18.51	−101.17	64	5.4	—	5[b]
29	2006/08/11	18.48	−101.18	64	4.9	—	5[b]
31	2006/08/17	18.72	−102.47	60	4.6	—	5[c]
32	2006/10/14	19.34	−103.50	43	4.0	—	5[c]
42	2006/12/17	18.10	−101.08	66	4.7	—	3
45	2006/12/27	18.43	−103.15	41	4.1	—	4
48	2007/02/06	18.12	−100.69	65	4.4	—	3
49	2007/02/11	21.41	−106.27	47	5.1	—	3
53	2007/03/08	19.09	−102.30	78	4.1	—	4
57	2007/03/31	16.90	−99.91	42	4.4	314/86/119	6
60	2007/04/28	16.96	−99.79	40	4.8	307/75/118	6
62	2007/05/28	19.18	−104.51	42	4.0	—	4
D3	2007/03/13	18.62	−101.60	85	4.1	—	3
D4	2007/03/08	19.09	−102.30	79	4.1	—	4
D5	2007/02/03	18.61	−101.48	72	4.3	—	5[c]

[a]Sources are 1) location, focal mechanism, M_w, and depth from the Global CMT catalog; 2) focal mechanism, M_w, and depth from V. Andrews (personal communication, 2010), location from CMT; 3) location, m_b, and depth from the Bulletin of the International Seismological Centre (ISC); 4) location, M_D, and depth from the Servicio Sismològico Nacional (SSN) catalog; 5) location, magnitude, and depth from the National Earthquake Information Center (NEIC); 6) focal mechanism, M_w, and depth from *Pacheco and Singh* [2010], location from ISC.
[b]m_b.
[c]M_D.

instruments deployed from January 2006 to June 2007 in a 2D geometry in the Jalisco and Michoacan regions with an average station spacing of ∼40 km (Figure 1). The goal of the MARS experiment was to understand the forces that are controlling the tectonics of the Jalisco block and the behaviors of the Rivera and adjacent Cocos plates [*Yang et al.*, 2009]. In this study, we analyze seismograms from 24 regional intraslab earthquakes recorded by the MARS array. These events are within the magnitude range of 4.0 to 6.2, and the depths vary from 40 km to 85 km (Table 1). The locations of these events are shown in Figure 1.

2.2. 1D Velocity Modeling

[7] The shallow seismic structure of the central Mexico subduction zone is analyzed in 1D using frequency-wave number forward modeling techniques. The sensitivity of observed waveforms to the subduction zone structure is tested using five different P- and S-wave velocity models: (1) standard Southern California (SoCal) crustal velocity model from *Dreger and Helmberger* [1993] (Figure 2a); (2) modified SoCal model with thickened crustal layers (SoCalx) to place the Moho at 45 km depth (Figure 2b); (3) central Mexico velocity model from receiver function study along the MASE array by *Kim et al.* [2010] (Figure 2c); (4) central Mexico velocity model from waveform modeling study along the MASE array by *Song et al.* [2009] (Figure 2d); (5) new central Mexico (ncM) velocity model from this study (Figure 2e). The SoCal and SoCalx models do not include slab structure, while the other models contain a multilayered, somewhat complex slab that includes the USL that was imaged by the MASE array (Figure 2). *Kim et al.*'s [2010] receiver function results are used to constrain the depth of the Moho to 45 km in the SoCalx and ncM models. The overriding plate velocities in the ncM model are taken from the *Song et al.* [2009] model, with the crustal layers thinned to place the Moho at the constrained depth (Figure 2e). The subducted plate structure in this model is modified from *Kim et al.* [2010] and consists of a 3 km thick USL atop a 3 km thick lower oceanic crust and a 4 km thick high velocity layer, overlying oceanic mantle (Figure 2e). The SoCal and SoCalx crustal models test the sensitivity of the observed waveforms to the crustal structure only, while the *Kim et al.* [2010] model tests waveform sensitivity to the slab structure only. The *Song et al.* [2009] and ncM models test the sensitivity of the observed waveforms to combined crustal and slab structure. The SoCal and SoCalx models were selected for their robust representations of simple crustal structure, not for their affinities with Mexican subduction zone structure.

[8] A comparison of the synthetics produced for each of these five models to the data for event 3 at three stations is shown in Figure 3. The waveforms have been bandpass filtered to 0.01–0.1 Hz in order to increase the signal-to-noise ratio and accentuate the major phases (e.g., P, sP, S, multiple S). Overall, the ncM model provides the most accurate prediction of the data, with the best fits to P, sP, and SH phases at all distances, along with an S-wave multiple at large distances (Figures 3 and 4). The SoCal model provides a comparable fit to these phases, but fails to predict some of the waveform complexities seen in both the data and the ncM model synthetics, such as the shoulder following SV (Figure 3). The uppermost slab structure in the ncM model, particularly the USL, is likely responsible for reproducing the observed waveform complexities that the simpler SoCal model fails to predict. The complete 1D

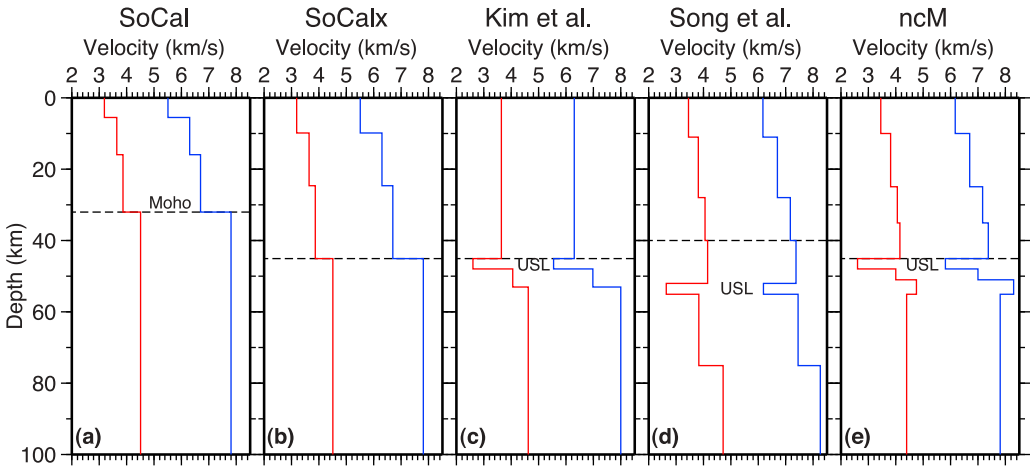

Figure 2. 1D P (blue) and S (red) wave velocity models tested in this study. (a) Southern California velocity model [*Dreger and Helmberger*, 1993]. (b) Modified southern California model with thickened crustal layers that place the Moho (black dashed line) at 45 km depth. (c) Central Mexico velocity model from receiver function study by *Kim et al.* [2010] using the MASE array. Ultra-slow velocity layer (USL) is indicated at the top of the subducted plate. (d) Central Mexico velocity model from waveform modeling study along the MASE array by *Song et al.* [2009]. (e) New central Mexico (ncM) velocity model from this study.

modeling results for the SoCal, SoCalx, *Kim et al.* [2010], and *Song et al.* [2009] velocity models are shown in Figures S1–S4 of the auxiliary material, respectively.[1]

[9] A NW-SE trending profile across the MARS array (see Figure 1 for location) of the ncM modeling results for event 3 illustrates some lateral variation in the structure of this region (Figure 5). For the stations located within the TMVB, complexities in the waveforms are observed after the arrival of the S-wave in the data and are most prevalent on the transverse component. These complexities are not predicted by the ncM model synthetics and may be indicative of a change in crustal structure within the TMVB region.

2.3. Ultra-slow Velocity Layer

[10] The USL atop the flat Cocos slab was imaged as a thin, 3–5 km thick layer with a V_P of 5.4–6.2 km/s and a V_S of 2.0–3.4 km/s [*Song et al.*, 2009; *Kim et al.*, 2010]. For the ncM model, we set these parameters to 3 km thick, V_P of 5.8 km/s, and V_S of 2.6 km/s. The exact nature of the USL is not known, but its anomalously low shear wave velocity suggests a relationship with fluids, specifically free water or hydrous minerals, in the subduction zone. *Song et al.* [2009] proposed that the USL represents part of the oceanic crust that is fluid-saturated, forming a high pore fluid pressure (HPFP) layer that is sealed by some low permeability layer, possibly fine-grained blueschist, directly above it. In their thermal modeling of the central Mexico subduction zone, *Manea et al.* [2004] found a high pore pressure ratio of 0.98 along the subduction interface, consistent with *Song et al.*'s [2009] HPFP layer, based on the extent of the coupled zone (450°C isotherm) from the trench. *Kim et al.* [2010] proposed that the USL is upper oceanic crust that is highly heterogeneous and composed of mechanically weak hydrous minerals (talc) that might be under high pore pressure. The hydrous minerals or high pore pressure of the USL is a likely explanation for the observed decoupling of the flat slab from the overriding plate, as evidenced by the lack of compressional seismicity in the North American plate [*Singh and Pardo*, 1993] and GPS observations [*Franco et al.*, 2005], and may be responsible for the flat subduction geometry, shown to be facilitated and sustained by such a low strength layer [*Manea and Gurnis*, 2007; *Kim et al.*, 2010].

[11] The presence of the USL atop the Cocos slab is identified by the existence of complex P waveforms [*Song et al.*, 2009] recorded by the MARS array. These complex P waveforms consist of three locally converted S-to-P phases (A, B, C) that arrive within 4 sec after the P-wave (Figure 6). Phase A converts at the bottom of the USL and appears as a negative pulse at local stations. Phase B arrives immediately after phase A as a positive pulse, indicative of an S-to-P wave that converted at the top of the USL. Phase C converts at the bottom of the high velocity layer, arriving before phase A and ~1.0–1.5 sec after the direct P-wave. These three phases are searched for on the recordings of the intraslab earthquakes analyzed in this study. P waveforms on these recordings are categorized as complex, possibly complex, or simple based on the existence or absence and nature of phases A, B, and C. Examples of these waveforms from event 1 are shown in Figure 6. The waveforms have been bandpass filtered to 0.01–0.6 Hz, with the shorter periods in the frequency band allowing for the identification of the three S-to-P phases. When all three of the phases are clearly visible, the waveform is deemed complex. If one of the phases is not easily identified due to an uncharacteristic pulse shape and/or amplitude, but the other two phases are clearly present, then the waveform is possibly complex. Simple waveforms lack the shoulder in the direct P pulse indicative of the C phase and also have uncharacteristically shaped and/or low amplitude A and B phases. These features of the simple P waveforms indicate there is no USL present.

[1]Auxiliary materials are available in the HTML. doi:10.1029/2012JB009528.

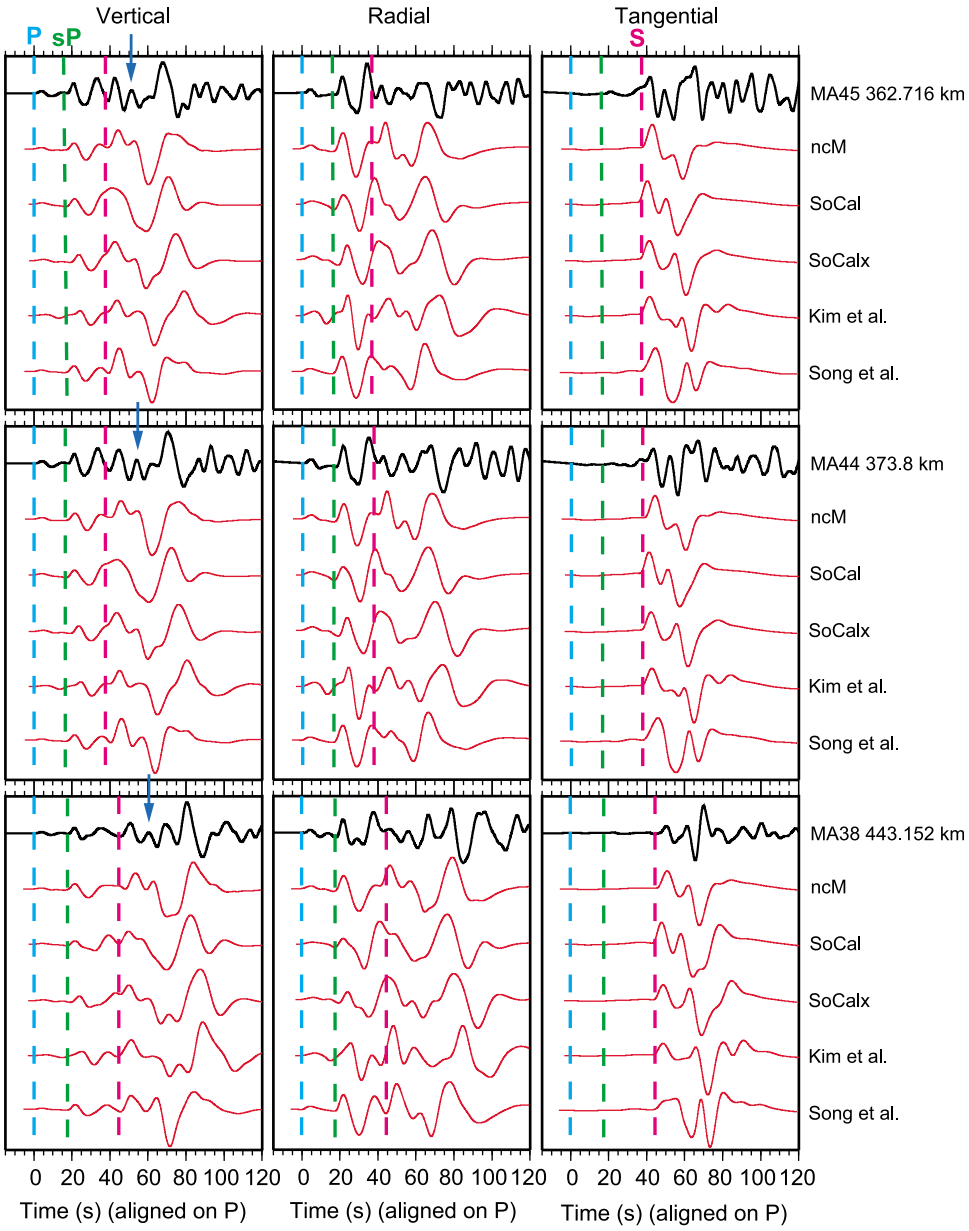

Figure 3. Comparison of 1D modeling results of event 3 for the five models tested at three stations. Waveforms are filtered to 0.01–0.1 Hz. Data are in black, synthetics are in red. P, sP, and S phases are indicated by dashed lines. Blue arrows indicate the shoulder following SV. Of the 1D models tested, ncM is preferred because it produces synthetics that accurately predict the waveshapes and arrival times of the P, sP, S, and SV shoulder phases in addition to the arrival time of the S-wave multiple. This model, however, fails to predict the waveshape of the S multiple and some post S multiple complexities, necessitating the development of a 2D model.

[12] The lateral extent of the USL is examined by mapping the locations of the S-to-P conversion points from the top of the Cocos slab for the eight events which exhibited complexity in their P waveforms (Figure 7). The locations of these conversion points are estimated using the TauP Toolkit [*Crotwell et al.*, 1999] with the ncM velocity model. The intermingling of S-to-P conversion points for stations that recorded complex, possibly complex, and simple P waveforms indicates that the USL is likely laterally heterogeneous, consistent with the observations of *Song et al.* [2009] and *Kim et al.* [2010]. An approximate location for the western edge of the USL atop the slab is proposed based on the locations of these conversion points. This edge is located between the conversion points for the westernmost event which exhibited P complexity (event 19) and the nearest neighboring event which produced simple waveforms (event 2). The USL edge is arbitrarily mapped as a linear feature normal to the trench, but its exact orientation or curvature may vary. This boundary of the USL is approximately coincident with the western margin of the projected OFZ region.

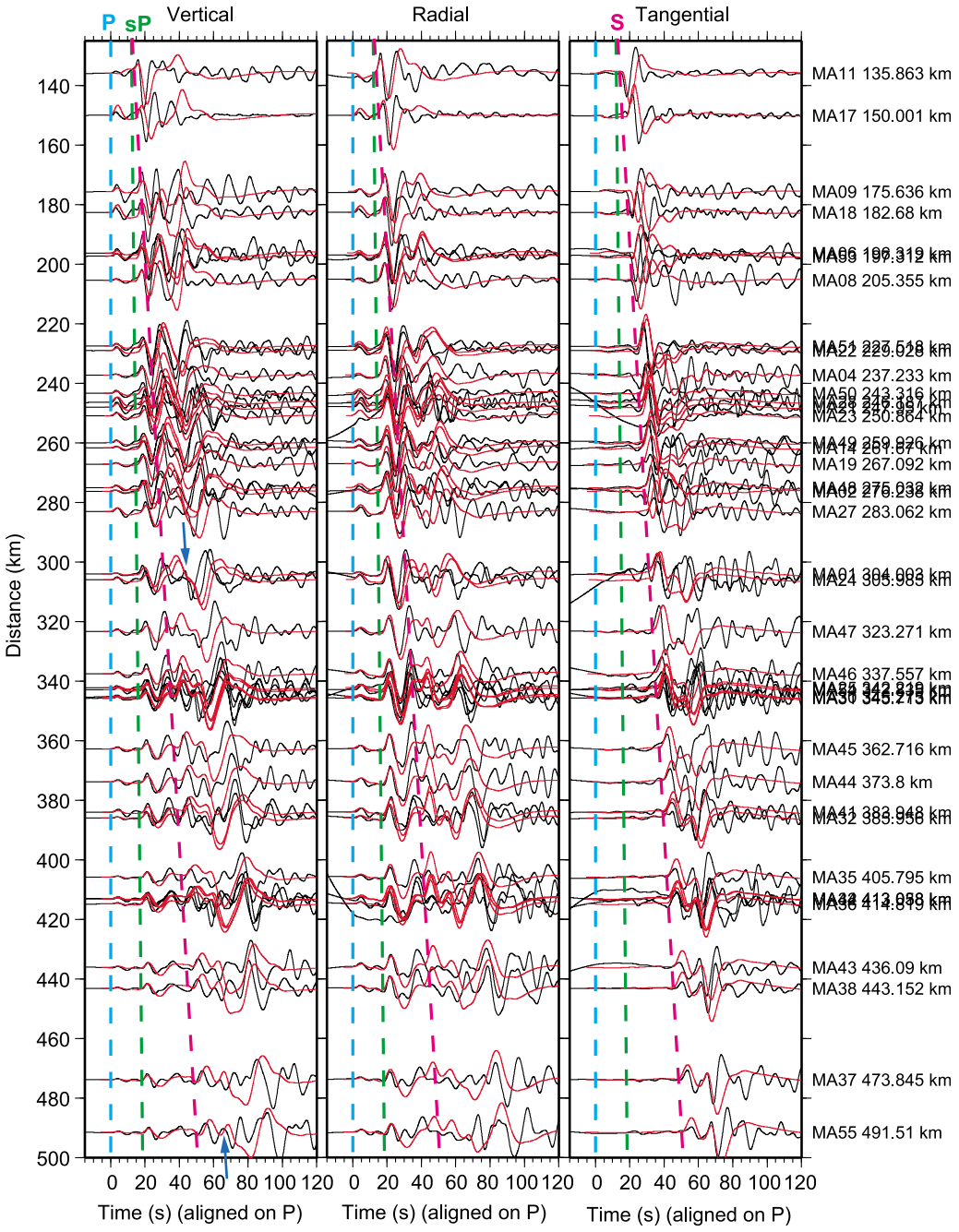

Figure 4. 1D modeling results of event 3 for the ncM velocity model filtered to 0.01–0.1 Hz. Data and synthetics are as in Figure 3. P, sP, and S phases are indicated and are predicted well by the ncM model. Blue arrows indicate the shoulder following SV.

2.4. 2D Velocity Modeling

[13] To further investigate the shallow structure of the subducted Rivera and Cocos plates, we produce synthetic seismograms with a 2D finite difference wave propagation algorithm for particular velocity and slab geometry models and compare these to the data for event 3 (the largest magnitude event). The preferred model is a NW-SE oriented profile across the MARS array (see Figure 1 for profile location) consisting of P- and S-wave velocities from the ncM model and subducted slab geometries estimated from the isodepth contours of *Pardo and Suárez* [1995] (Figure 8). The USL in this model ends at the approximate edge location. The synthetics produced from this model are compared to the data in Figure 9. The model predicts the P and sP phases reasonably well at all distances and the S-wave at most distances. A later large amplitude phase, presumed to be an S-wave multiple, is predicted reasonably well by the model at distances greater than ~320 km.

[14] In order to test the effect of the presence or absence of the USL, the location of its edge, and the geometry of the subducted slabs on the synthetic seismograms produced, we examine four other models with the same velocity structure:

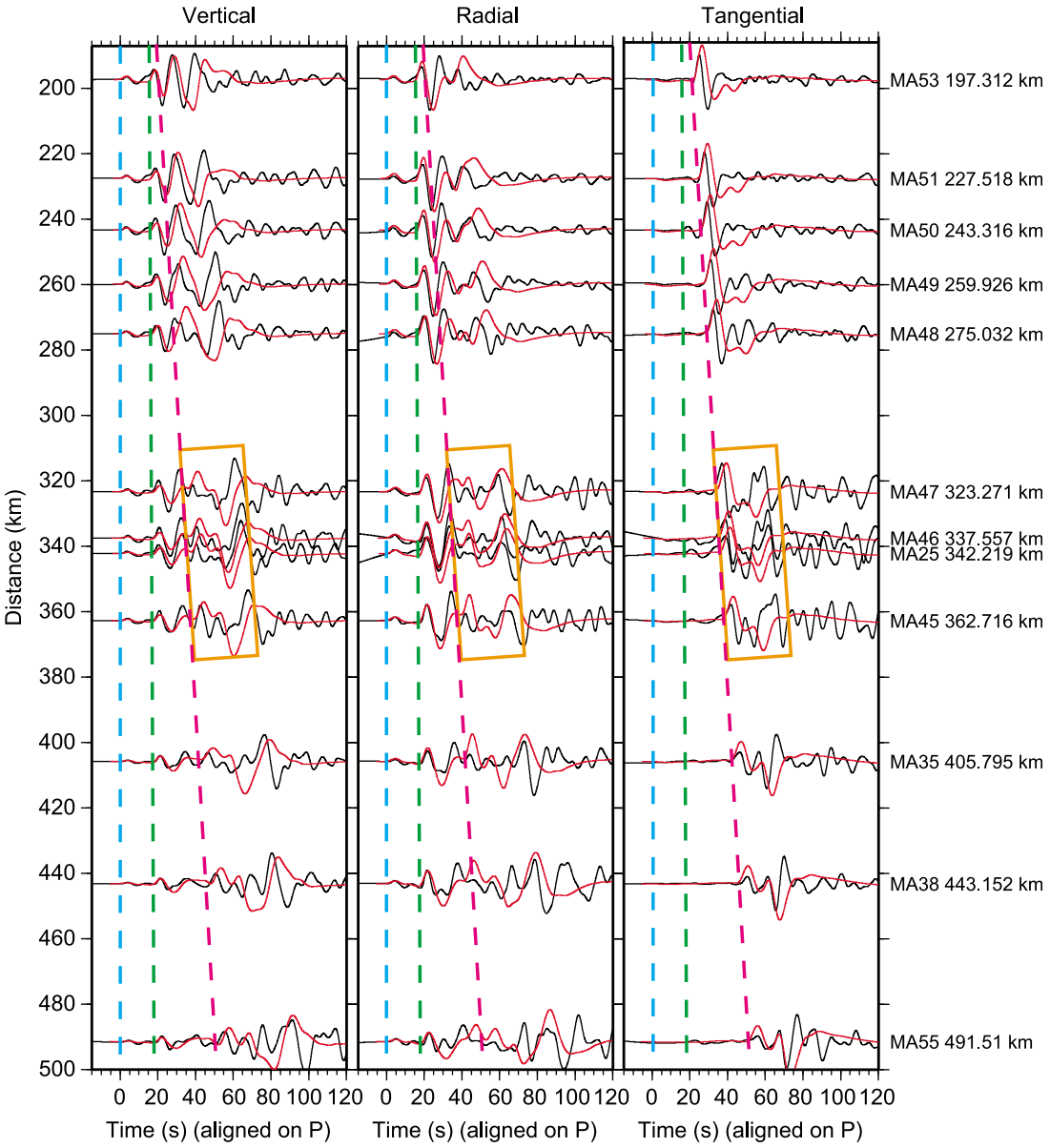

Figure 5. Profile across the MARS array along the NW-SE line in Figure 1. Data and synthetics are as in Figure 3. For the stations located within the TMVB, complexities in the waveforms are observed after the arrival of the S-wave in the data (indicated by orange box) and are not predicted by the model.

(1) no USL, but a thicker lower oceanic crust layer to maintain overall slab thickness (no USL); (2) USL continues across entire width of model without an edge (full USL); (3) USL edge shifted 100 km to the northwest (edge + 100); (4) USL edge at approximated location, but subducted Rivera slab geometry is horizontal (or flat) northwest of the TMVB (edge fltRiv). We tested a variety of shift amounts for the edge +100 model (−30 km, −20 km, −10 km, +10 km, +20 km, +30 km, +40 km, +50 km, +100 km), but found no appreciable difference in the synthetics produced for shifts <100 km when compared to the edge model (i.e., unshifted) synthetics. A comparison of the synthetics produced for each of the four models and the preferred (edge) model to the data at four stations is shown in Figure 10. A ∼48 sec segment of the waveform after the S-wave that includes the large amplitude, presumed S-wave multiple illustrates the greatest variance among the models, indicating this phase is most sensitive to the USL. The synthetic waveform for each model is cross-correlated with the data for this segment. The insignificant difference in correlation coefficients for the edge and edge fltRiv models show that the shape of the subducted Rivera slab is poorly resolved in our preferred model. While there is some variance between the vertical and radial components, in general, the correlation coefficients indicate that the edge model synthetics are better representations of the data than the no USL and full USL models. The correlation coefficients for the majority of the twelve stations located along the profile clearly indicate that the edge model synthetics fit the data better than those produced by the edge +100 model. In Figure 10, this finding is illustrated at stations MA45, MA48, and MA49 (radial component), while at station MA25, an exception to

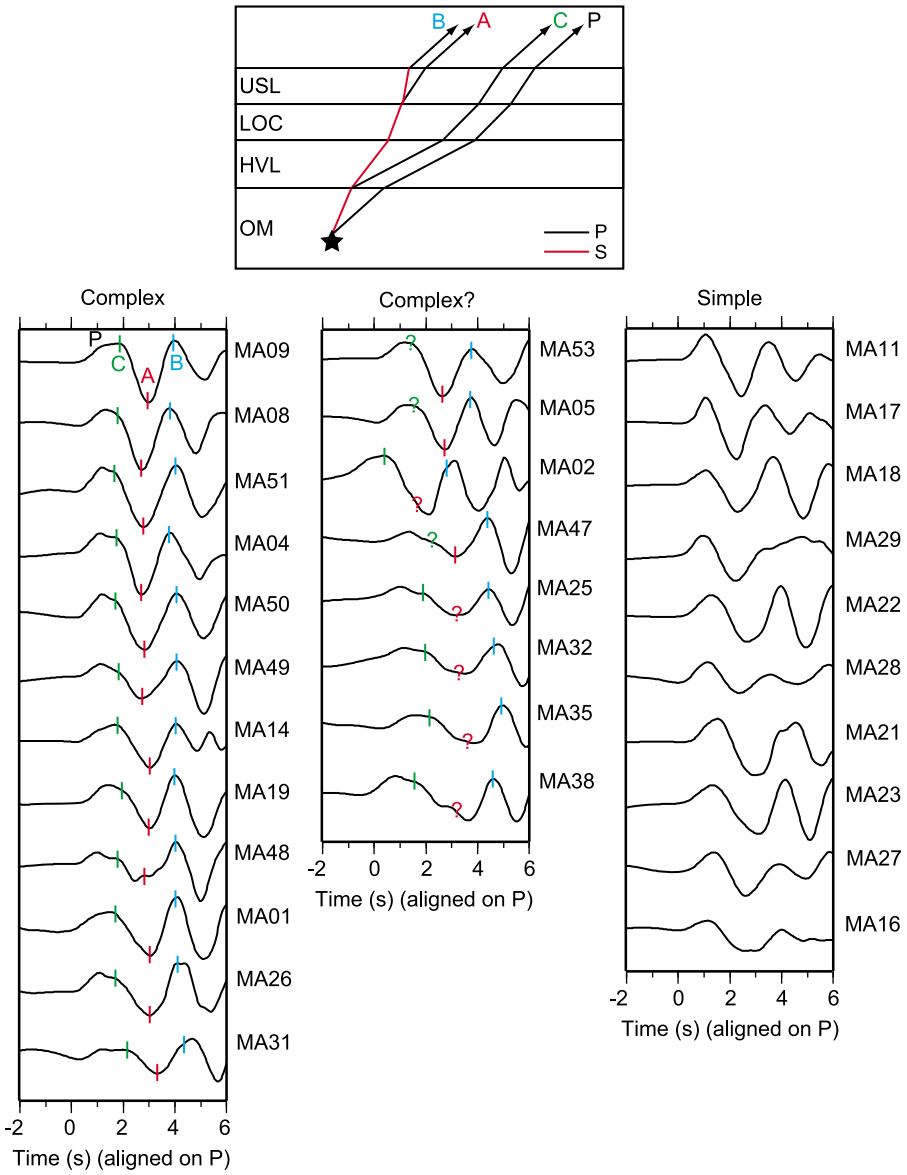

Figure 6. (top) Schematic illustrating the raypaths of the P-wave and the three S-to-P phases (A, B, C) that comprise the complex P waveform. Abbreviations are USL, ultra-slow velocity layer; LOC, lower oceanic crust; HVL, high velocity layer; OM, oceanic mantle. (bottom) Examples of (left) complex, (middle) possibly complex, and (right) simple P waveforms from event 1 recorded on the vertical component and filtered to 0.01–0.6 Hz. S-to-P phases A, B, and C are indicated by red, blue, and green tick marks, respectively. All three of these phases are visible in the complex waveforms within 4 sec of the P-wave. Question marks on the possibly complex waveforms indicate a phase that is not easily identified due to an uncharacteristic pulse shape and/or amplitude. Simple waveforms lack the shoulder in the direct P pulse indicative of the C phase and also have uncharacteristically shaped and/or low amplitude A and B phases, indicating there is no USL present.

this result, the edge +100 model more accurately predicts the data.

2.5. Seismicity and Slab Dip Across USL Edge

[15] The variation in slab dip across the USL edge is examined in detail to locate any abrupt changes in geometry which could be indicative of a possible plate boundary. Epicenters for earthquakes located between 16.5°N and 20.5°N from the January 2001–May 2011 event catalog of the Servicio Sismológico Nacional (SSN) are mapped and divided into four 50 km wide trench normal bins parallel to the USL edge (Figure 11a). The locations of events furnished by the SSN have been carefully revised by an analyst and checked against the locations provided by the Global Centroid Moment Tensor (GCMT) and National Earthquake Information Center (NEIC) catalogs [*Noriega-Manzanedo and Pérez-Campos*, 2010]. Bins 1 and 2 are located east of the USL edge and include the majority of the projected OFZ region. Bins 3 and 4 are located west of the USL edge. There is a significant decrease in the seismicity in the western bins compared to the eastern bins,

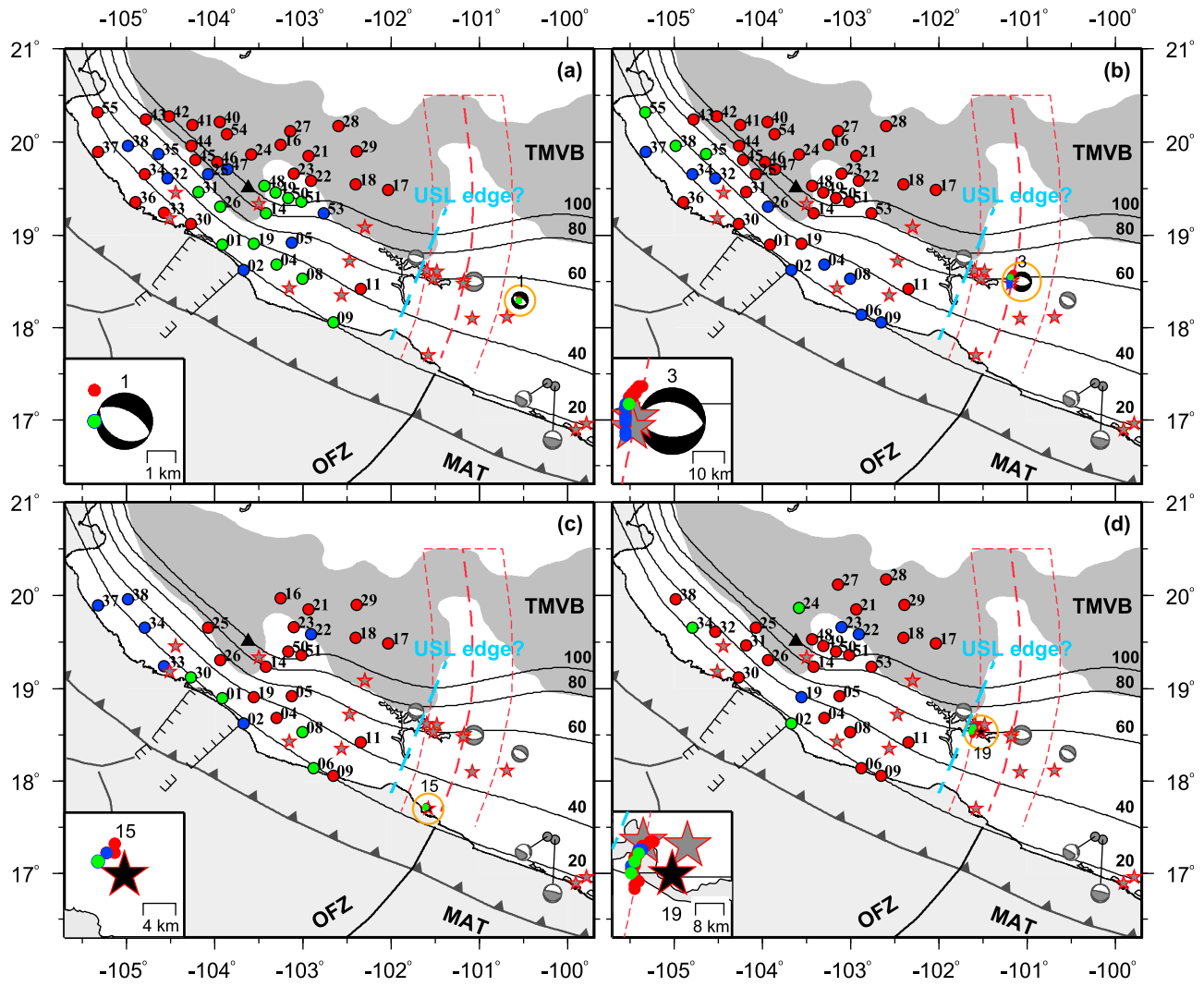

Figure 7. Local S-to-P conversion points from the top of the Cocos slab (small dots) for MARS stations which recorded complex (large green dots), possibly complex (large blue dots), or simple (large red dots) P waveforms for eight events which exhibited complexity (conversion points are colored corresponding to station). An approximate location for the western edge of the USL atop the slab is proposed (blue dashed line) based on the locations of these conversion points. The events shown are (by event number) (a) 1, (b) 3, (c) 15, (d) 19, (e) 28, (f) 29, (g) 42, and (h) 48. The location of each of these events is shown in black and highlighted with an orange circle. Insets show enlarged view of event and conversion point locations. Other events are shown in grey.

which is indicative of a structural change across the USL edge. Cross-sections of the seismicity in each bin illustrate variations in the Benioff zone across the region and are used to estimate the slab dip in each bin (Figure 11b). The dip angle is estimated by visually selecting hypocenter locations that are downdip of the trench and are not within the overriding plate, then performing a linear regression of the selected locations. There is a considerable difference in slab dip between bins 1 (25°) and 2 (39°), while the slab dip is constant across bins 3 and 4 (41°) (Figure 11c). Using an estimated maximum error of ±5° for each bin, the errors on these dip estimates are weighted by the number of earthquakes in each bin, such that fewer events in a bin produces a larger error, with values ranging from ±2.5° (bin 1) to ±4.5° (bin 4). These dip estimates indicate a significant change in slab geometry across the projected OFZ region, which the USL continues through, and constant geometry west of the USL edge.

3. Discussion

[16] Previous evidence suggestive of the ongoing fragmentation of the Cocos plate has been purely tectonic in nature, while in this study we provide evidence based on seismic observations and modeling of the velocity structure of the central Mexico subduction zone. From mapping the locations of S-to-P conversion points, we find the location of the USL edge to be approximately coincident with the western margin of the projected OFZ region. Although indicated as a linear feature, we have minimal constraints on the orientation and shape of the USL edge due to limited earthquakes in the

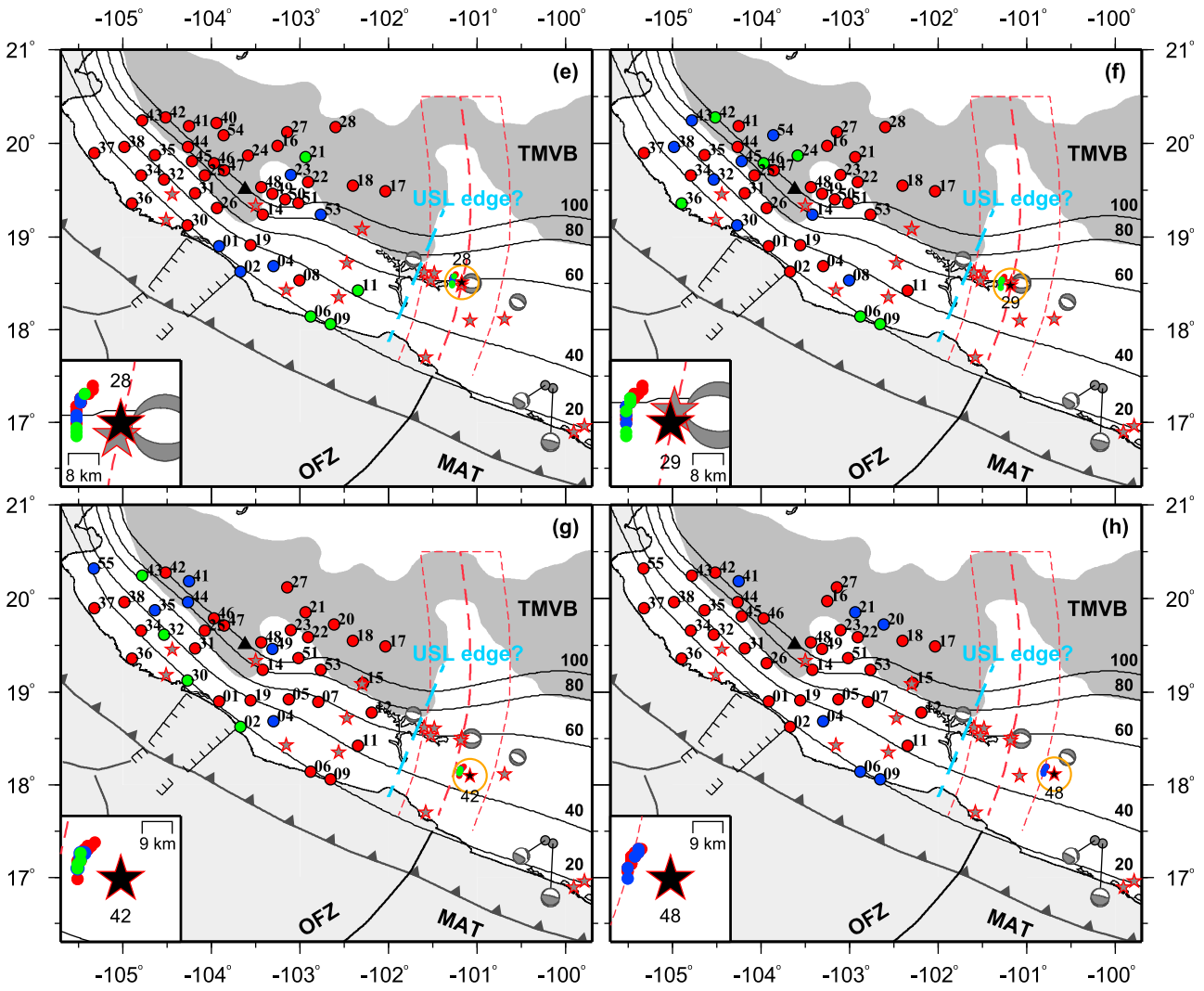

Figure 7. (continued)

region, so it is possible that it could instead follow a curved path parallel to the projected OFZ. The 2D finite difference modeling confirmed the location of the USL edge where it intersects the NW-SE profile across the MARS array. The coincidence of the confirmed USL edge with the western margin of the projected OFZ region indicates that this margin is a sharp structural boundary. On the basis of these results, we propose a slab tear model, wherein the Cocos slab is currently fragmenting into a North Cocos plate and a South Cocos plate along the projection of the OFZ by a process similar to that which occurred when the Rivera plate separated from the proto-Cocos plate (Figure 12). The presence and location of this slab tear are consistent with the anisotropy pattern found by *Stubailo et al.* [2012] using Rayleigh wave phase velocity dispersion measurements. The continuation of the USL across the projected OFZ region indicates that the N Cocos and S Cocos slabs are not currently separated by a significant gap, but rather that the OFZ region may be acting as a transition zone [*Blatter et al.*, 2007] in this young tear. This is contrary to the mature tear along the Rivera-Cocos plate boundary where a distinct gap between the slabs has been observed [*Yang et al.*, 2009].

[17] The variations in observed seismicity and slab dip across the USL edge from the SSN catalog data provide further evidence for a distinct N Cocos-S Cocos plate boundary along the western margin of the projected OFZ region and can be used to explain why the USL terminates here. The S Cocos seismicity bins (1 and 2) overly the OFZ and contain more than three times the events in the N Cocos bins (3 and 4). This large variation in observed seismicity on either side of the USL edge indicates that this is a marked structural boundary. The observed change in slab dip across the S Cocos bins and the constant slab dip across the N Cocos bins is consistent with the interpretation that the OFZ region is a transition zone of changing geometry, while the N Cocos exhibits stable geometry. This result also signifies that the USL edge is a distinct structural boundary, which we interpret as the N Cocos-S Cocos plate boundary. Based on this interpretation, the OFZ transition zone is structurally S Cocos, which explains why the USL ends along its western margin. If the presence of

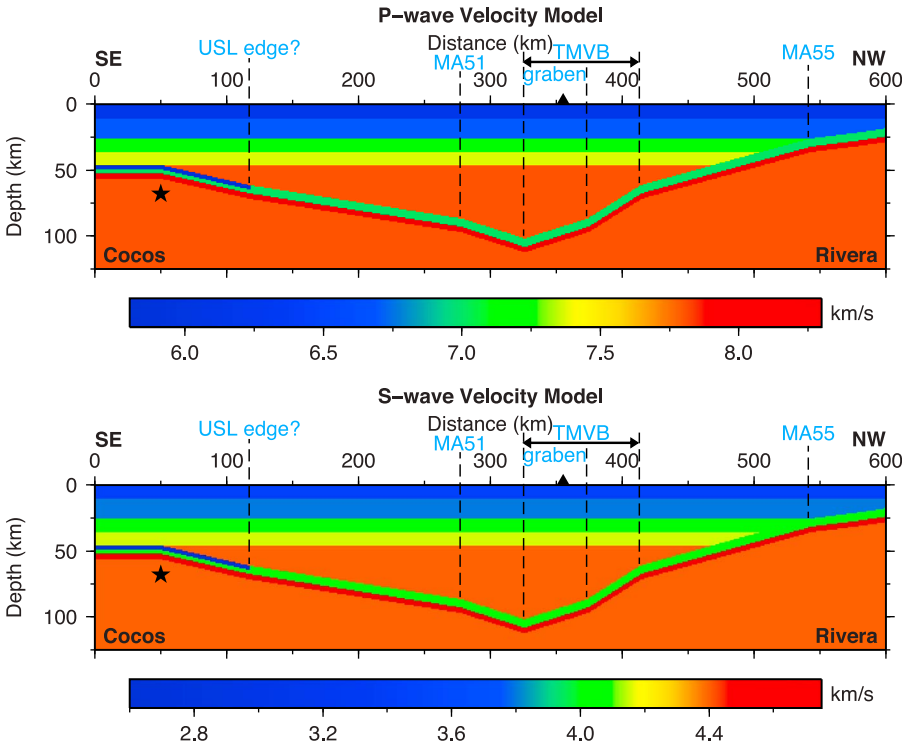

Figure 8. 2D velocity model of the shallow subduction zone structure across the MARS array along the NW-SE profile in Figure 1. P- and S-wave velocities are from the ncM model. Subducted slab shape is estimated from the isodepth contours of *Pardo and Suárez* [1995]. Locations of the approximate USL edge, stations MA51 and MA55, Colima graben, TMVB, and Colima volcano (black triangle) are indicated for reference. The location of event 3 used in the modeling is shown by the black star.

the USL was controlled simply by slab geometry, then we would expect its lateral extent to lie along the eastern margin of the projected OFZ region where the slab ceases to underplate the North American plate in a flat geometry. The low permeability fine-grained blueschist cap layer of *Song et al.* [2009] would likely be lost as the slab dip increased and the subsequently larger pressures and temperatures of the subduction zone metamorphosed the blueschist to coarse-grained eclogite, which would not be capable of sealing the water in the HPFP USL. As the USL continues across the transition from flat to normal subduction and across the OFZ, its lateral extent is clearly not controlled by a change in geometry. The USL appears to be purely a feature of the S Cocos plate with the location of its edge caused by the end of the S Cocos slab at the N Cocos-S Cocos plate tear along the western margin of the projected OFZ region. The USL ends due to the structural change from one plate to another, which may be related to the tear itself. It can be theorized that the plate tear breaks the USL, allowing entrained water from the hydrous minerals and/or pore spaces to be released, which effectively prevents the USL from continuing.

[18] The fragmentation of a lithospheric plate, such as the Cocos plate, along a fracture zone can be related to the subduction and inherent structure of the fracture zone itself. A fracture zone is usually of lower density than the surrounding oceanic plate and, as such, it tends to resist subduction or subduct in a different way [*Chung and Kanamori*, 1978; *Rosenbaum et al.*, 2008; *Blatter and Hammersley*, 2010], modifying the geometry of the subduction zone [*Vogt et al.*, 1976; *McCann and Habermann*, 1989; *Franke et al.*, 2008]. This increased resistance against subduction due to buoyancy coupled with the bathymetric relief of the fracture zone likely enhances downdip extensional stress in the slab [*Chung and Kanamori*, 1978] and increases vertical and horizontal stresses on the overriding plate, creating or reactivating preexisting fractures [*McCann and Habermann*, 1989]. The subduction of a fracture zone causes some degree of local decoupling of the oceanic plate from the overriding plate and/or creates a zone of extension within the slab [*Eissler and Kanamori*, 1982; *Huchon and Bourgois*, 1990], illustrating its nature as a weaker interface compared to the surrounding lithosphere [*Lowrie et al.*, 1986; *Kostoglodov and Ponce*, 1994; *Hall and Gurnis*, 2005; *Lonsdale*, 2005; *Porritt et al.*, 2011]. A fracture zone, as a line of weakness, is therefore an ideal place for a lithospheric tear to develop, resulting in the fragmentation of the subducted oceanic plate into distinct segments, each behaving as an individual unit [*Sillitoe*, 1974; *Vogt et al.*, 1976; *Nixon*, 1982; *Burbach et al.*, 1984; *Lonsdale*, 1991; *Rosenbaum et al.*, 2008; *Sigloch*, 2011]. The proposed fragmentation of the Cocos plate along the OFZ is an example of this process. The tectonic history of the northeast Pacific supports this theory of the OFZ as a plate boundary. From about 11 Ma to 6.5 Ma, the OFZ was the location of the Rivera-Cocos plate boundary before the Pacific-Rivera spreading center migrated northward and the Pacific-Cocos spreading center jumped north to the Rivera Fracture Zone (RFZ) [*Klitgord and Mammerickx*, 1982; *Mammerickx and Klitgord*, 1982]. As a previously active plate boundary, it is certainly

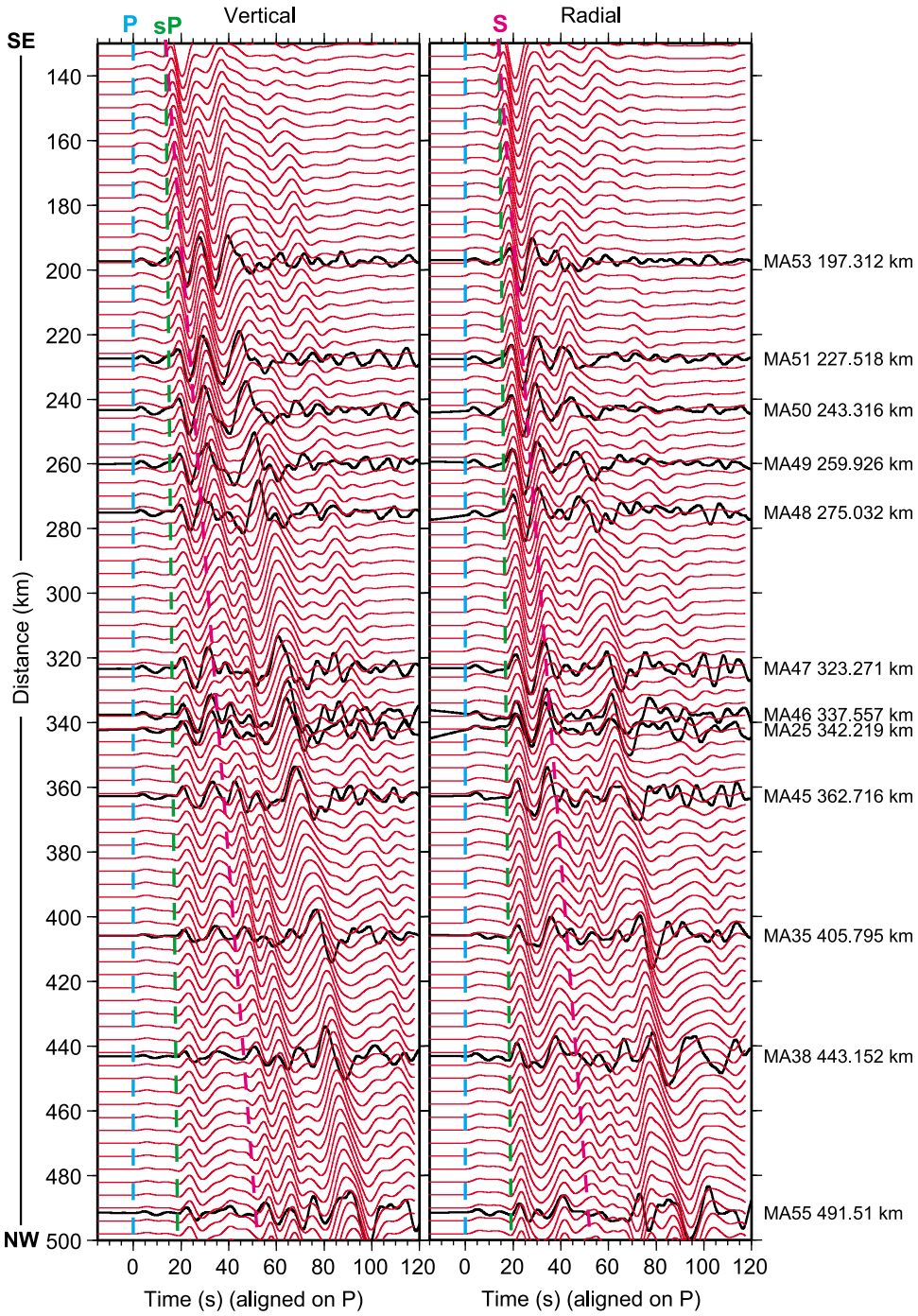

Figure 9. 2D modeling results of event 3 along the NW-SE profile filtered to 0.01–0.1 Hz. Data are in black, synthetics are in red. P, sP, and S phases are indicated.

possible and highly feasible for the OFZ to become reactivated as a plate boundary with the fragmentation of the Cocos plate.

[19] A fracture zone like the OFZ reflects discontinuities in the underlying subduction zone [*Sillitoe*, 1974; *Lowrie et al.*, 1986; *Lonsdale*, 1991; *Hall and Gurnis*, 2005; *Porritt et al.*, 2011] such as contrasting lithosphere age, buoyancy, slab dip, topography, and convergence rate, which can be used to explain the plate tearing process. The age of the lithosphere at the OFZ is 17.6 Ma on the N Cocos and 14.5 Ma on the S Cocos [*Pardo and Suárez*, 1995]. The older, colder, and therefore, denser N Cocos slab subducts at a steeper angle than the younger, more buoyant S Cocos slab which is nearly horizontal [*Blatter et al.*, 2007; *Blatter and Hammersley*, 2010]. This drastic change in slab dip (~10–15° to ~30°) [*Pardo and Suárez*, 1995] could be contributing to the tearing along the OFZ, although *Pardo and Suárez* [1995] argue for smooth contortions between these geometries, rather than tear faults. The convergence rate on either side of the OFZ is a constant 5.6 cm/yr, but this rate slows to the north and speeds up to the south [*DeMets et al.*, 1990], indicating an

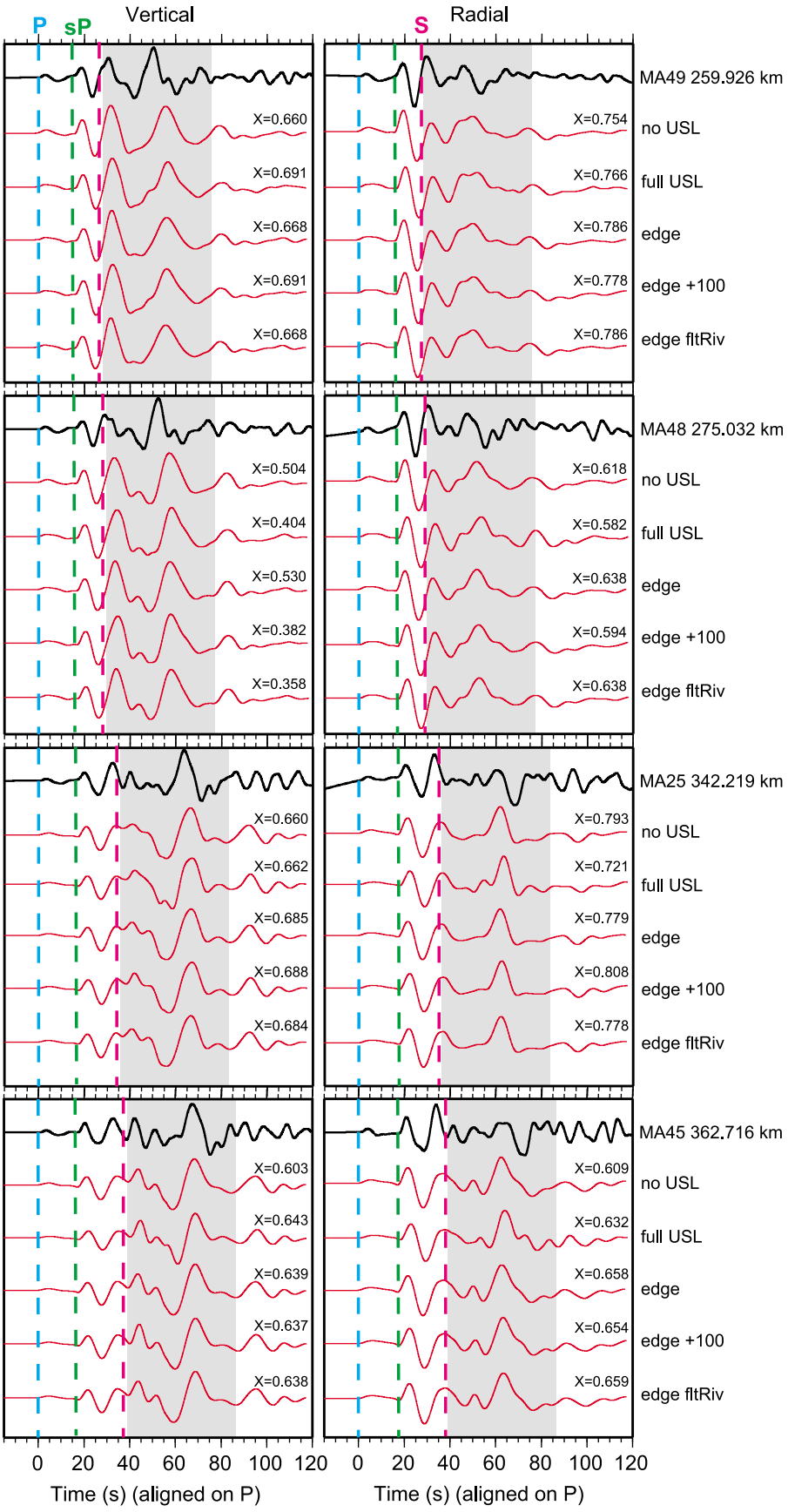
P
sP
Vertical
S
Radial
MA49 259.926 km
X=0.660
X=0.691
X=0.668
X=0.691
X=0.668
X=0.754
X=0.766
X=0.786
X=0.778
X=0.786
no USL
full USL
edge
edge +100
edge fltRiv
MA48 275.032 km
X=0.504
X=0.404
X=0.530
X=0.382
X=0.358
X=0.618
X=0.582
X=0.638
X=0.594
X=0.638
no USL
full USL
edge
edge +100
edge fltRiv
MA25 342.219 km
X=0.660
X=0.662
X=0.685
X=0.688
X=0.684
X=0.793
X=0.721
X=0.779
X=0.808
X=0.778
no USL
full USL
edge
edge +100
edge fltRiv
MA45 362.716 km
X=0.603
X=0.643
X=0.639
X=0.637
X=0.638
X=0.609
X=0.632
X=0.658
X=0.654
X=0.659
no USL
full USL
edge
edge +100
edge fltRiv
0 20 40 60 80 100 120
Time (s) (aligned on P)
0 20 40 60 80 100 120
Time (s) (aligned on P)

Figure 10

overall slower convergence rate for the N Cocos plate relative to the S Cocos. This slower convergence may be related to the rugged topography of the oceanic crust that was observed between the OFZ and the RFZ, relative to the smooth topography south of the OFZ [*Kostoglodov and Ponce*, 1994; *Ramírez-Herrera et al.*, 2011]. The rougher topography offers greater resistance to subduction, resulting in a slower convergence rate. This difference in resistance against the oceanic lithosphere to the north and south of the OFZ may result in differential motion between these two lithospheres [*Chung and Kanamori*, 1978; *Lonsdale*, 2005], leading to a tear. In *Wortel and Cloetingh*'s [1981, 1983] plate fragmentation model, the lateral variation in the age of the slab across the OFZ (~3 Ma) would produce significant tensional stresses in the plate, possibly causing fragmentation of the oceanic plate [*Burkett and Billen*, 2010]. These stresses would result from the variable slab pull forces and trench resistance forces which depend on the age of the subducting lithosphere, where slab pull forces are greater for older lithosphere and trench resistance forces are greater for young lithosphere [*Wortel and Cloetingh*, 1981, 1983]. If these tensional stresses exceed the strength of the lithosphere, then tearing or stretching of the plate may occur [*Wortel and Cloetingh*, 1981, 1983; *Burkett and Billen*, 2010].

[20] A special case of the more general plate fragmentation mechanism proposed by *Wortel and Cloetingh* [1981, 1983] is the process of pivoting subduction [*Menard*, 1978], which emphasizes the role of differences in the direction of motion rather than differences in the relative rate of motion between segments of a plate in the course of a fragmentation event [*Lonsdale*, 1991, 2005; *Bandy et al.*, 2000]. Pivoting subduction involves a pinned geometry in which a ridge and a trench approach one another obliquely and the young buoyant lithosphere near the point where they meet resists subduction so that the plate pivots about the point [*Menard*, 1978; *Burkett and Billen*, 2010]. This is the process by which the proto-Cocos plate fragmented into the Rivera and Cocos plates [*Bandy et al.*, 2000]. In response to the collision of the East Pacific Rise (EPR) with the MAT off the southern tip of Baja California [e.g., *Mammerickx and Klitgord*, 1982; *Atwater*, 1989; *Lonsdale*, 1991], a small part of the proto-Cocos plate near the point of collision began to pivot about a new pole located close to this point [*Bandy et al.*, 2000]. The motion of the remainder of the proto-Cocos plate to the south was unaffected by the ridge-trench collision, and this differing response of the two parts of the plate produced extensional stresses within the plate which resulted in a zone of extensional deformation, or tearing [*Burkett and Billen*, 2010] along the present Rivera-Cocos plate boundary [*Bandy et al.*, 2000]. Plate motions suggest that the stresses were greatest at the northeast extent of the subducted Rivera-Cocos boundary and the tearing propagated to the southwest toward the EPR [*Bandy et al.*, 1998, 2000; *Serrato-Díaz et al.*, 2004]. This extensional deformation along the Rivera-Cocos plate boundary is consistent with the location and formation of the Colima Graben and its offshore extension to the southwest, the El Gordo Graben. The propagation of tearing from northeast to southwest is also consistent with the seismic tomography images of *Yang et al.* [2009], which show a clear gap between the subducted Rivera and Cocos plates that widens in the downdip (northeast) direction.

[21] The Cocos plate is proposed to be fragmenting along the OFZ by a recently initiated (0.9 Ma) [*Bandy et al.*, 2000] pivoting subduction process analogous to that which occurred when the Rivera plate separated from the proto-Cocos plate. The wedge-shaped Cocos plate includes curved fracture zone traces, fanning magnetic anomalies [*Lynn and Lewis*, 1976; *Atwater*, 1989], and a Pacific-Cocos spreading rate that increases southward along the EPR [*Klitgord and Mammerickx*, 1982; *Atwater*, 1989]. The northern terminus of the Pacific-Cocos spreading center is approaching the MAT [*Bandy and Hilde*, 2000], with the pole of opening located nearby to the north [*Mammerickx and Klitgord*, 1982]. When all of these features are taken into account, it becomes clear that the present Cocos plate is a good approximation of the pinned geometry described by *Menard* [1978]. The younger, more buoyant lithosphere of the northern Cocos plate resists subduction and pivots about the nearby Pacific-Cocos pole, while the motion of the southern Cocos plate remains unchanged. This difference in the direction of motion of the two parts of the plate produces extensional stresses in the plate, which result in the ongoing tearing, or fragmentation, into a N Cocos plate and a S Cocos plate along the landward projection of the OFZ.

[22] There are several tectonic observations which support the theory that the Cocos plate is fragmenting along the OFZ by a process analogous to the Rivera-Cocos tear event. The variations in plate motions on either side of the boundary are one example of such an observation. *DeMets et al.* [1990] and *DeMets and Wilson* [1997] noted a systematic misfit of ~3 mm/yr of Pacific-Cocos spreading rates relative to magnetic anomalies from the EPR north of the OFZ. They attributed this misfit to seafloor north of the OFZ which moves relative to the rigid Pacific and Cocos plates. *Bandy et al.* [2000] report the results of a statistical F-Test which was performed to test for the presence of a N Cocos plate. This test passed at the 5% risk level, suggesting that the motion of the Cocos plate north of the OFZ is different than that to the south [*Bandy et al.*, 2000]. The 5°–9° change in strike of the Pacific-Cocos spreading center segment on either side of the OFZ further suggests that the motion of the Cocos plate changes at this boundary [*Bandy et al.*, 2000]. These observations of variable plate motions on either side of the OFZ indicate the presence of separate N Cocos and S Cocos plates, which are fragmenting from one another along the eastward projection of the OFZ. Evidence for this landward projection lies in the existence of an embayment in the TMVB along its path [*Blatter et al.*, 2007; *Blatter and*

Figure 10. Comparison of 2D modeling results for five different models at four stations. The primary variance among the models was the USL: no USL = no USL present, thicker lower oceanic crust to compensate; full USL = USL continues across entire width of model without an edge; edge = USL stops at approximated edge location; edge + 100 = USL edge shifted 100 km to the northwest; edge fltRiv = USL edge at approximated location, subducted Rivera slab shape made horizontal (or flat) northwest of the TMVB. Segment of waveform illustrating greatest variance among the models is shaded grey. Cross-correlation coefficients (X) for each model with the data for the selected segment are shown.

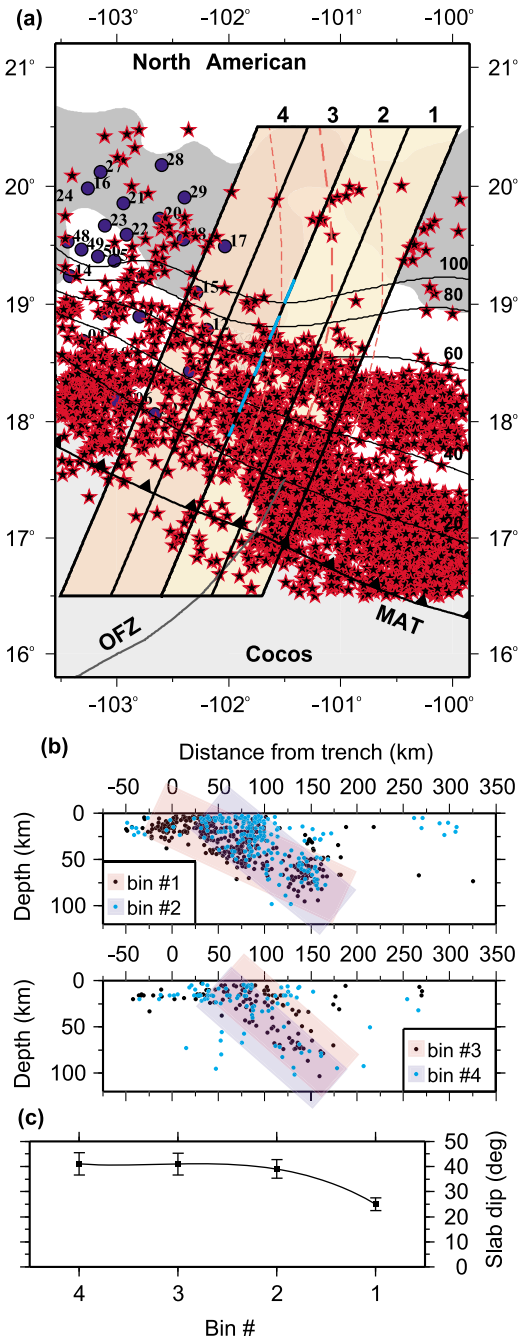

Figure 11. Seismicity and slab dip across the USL edge. (a) Map showing epicenters (stars) for earthquakes located between 16.5°N and 20.5°N from the 1/2001–5/2011 SSN catalog. Data in four 50 km wide bins parallel to the USL edge (blue dashed line) are analyzed for changes in slab dip across this region. Bins 1 and 2 (yellow) are on the South Cocos plate, and bins 3 and 4 (peach) are on the North Cocos plate. Note the decreased seismicity in bins 3 and 4 relative to bins 1 and 2. (b) Cross-sections of seismicity in the (top) S Cocos slab and (bottom) N Cocos slab. Note the significant change in slab dip between bins 1 and 2 and the constant slab dip across bins 3 and 4. (c) Plot of slab dip across the four data bins. Error bars are weighted by the number of events in each bin, such that fewer events produces a larger error.

Hammersley, 2010]. The subduction of fracture zones is known to produce an interruption or offset of a volcanic chain [e.g., *Sillitoe*, 1974; *Vogt et al.*, 1976; *Eissler and Kanamori*, 1982], such as that observed in the TMVB along the projection of the RFZ, or Rivera-Cocos plate boundary, [*Nixon*, 1982] and the Tzitzio Gap in the TMVB along the projection of the OFZ [*Blatter et al.*, 2007; *Blatter and Hammersley*, 2010].

[23] The observation of a possible rift-rift-rift triple junction overlying the projected OFZ region [*Bandy et al.*, 2000] provides further support for the fragmenting Cocos plate theory. This triple junction is comprised of broad river valleys [*Kostoglodov and Ponce*, 1994] with the eastern and southern rifts containing the Rio Balsas [*Ramírez-Herrera et al.*, 2011], the western rift containing the Rio Tepalcatepec, and Lake Presa del Infiernillo lying at their juncture [*Bandy et al.*, 2000]. This triple junction overlying the proposed zone of separation between the N Cocos and S Cocos plates is similar to the Colima-Chapala-Zacoalco rift-rift-rift triple junction which overlies the Rivera-Cocos plate boundary [*Bandy et al.*, 2000; *Bourgois and Michaud*, 2002]. The rifts of the Rivera-Cocos system contain the Colima Graben in the south, Lake Chapala in the east (part of the Chapala Graben), and the Zacoalco Graben in the northwest [*Luhr et al.*, 1985; *Allan*, 1986]. Both of these triple junctions reflect the response of the overriding plate to divergence of the plate below. In the Rivera-Cocos plate boundary case, the divergence is that between the Rivera and N Cocos slabs, while in the OFZ case, the divergence is that between the N Cocos and S Cocos slabs. The OFZ triple junction is of a smaller scale than that of the Rivera-Cocos boundary, with less developed rifts or grabens, indicative of the young age of the N Cocos-S Cocos plate tear relative to the mature Rivera-Cocos tear.

[24] The apparent tear along the OFZ may play an important role in the rollback dynamics of the slab in central Mexico. The age of volcanism north of Mexico City shows that the slab has been rolling back from 20 Ma to present [*Ferrari*, 2004]. This would necessitate trench parallel flow in order to move material from the backarc to the forearc [*Russo and Silver*, 1994; *Schellart et al.*, 2007; *Burkett and Billen*, 2010]. This flow is presumably currently accommodated by the tear between the Cocos and Rivera plates [*Soto et al.*, 2009]. A tear along the OFZ would significantly short-cut this process, and it may be that tearing is a natural part of this process.

4. Conclusions

[25] We have studied the seismic structure of the central Mexico subduction zone along the transition from flat to normal subduction using 1D and 2D waveform modeling techniques and an analysis of P waveform complexities. The results show that the subducted Cocos plate is a complicated, multilayered structure with a thin USL atop the slab. The lateral extent of this USL is approximately coincident with the western margin of the projected OFZ region, implying a structural boundary which we interpret as a tear in the Cocos plate. Recent tectonic observations in the region of variable plate motions on either side of the OFZ and a small-scale rift-rift-rift triple junction overlying the landward projection of the OFZ have suggested that the Cocos plate is

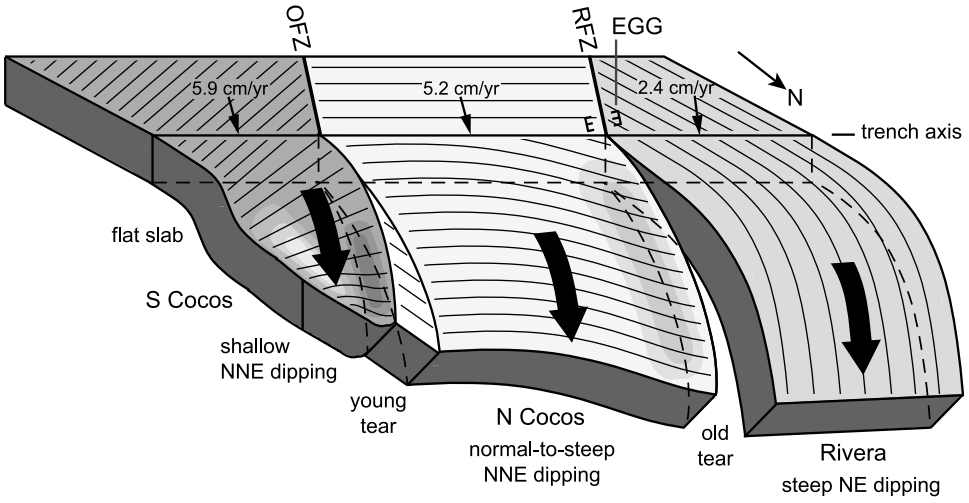

Figure 12. 3D schematic of the two-tear model illustrating the geometry of the S Cocos, N Cocos, and Rivera plates, along with the Orozco (OFZ; young tear) and Rivera (RFZ; old tear) fracture zones. Plate convergence rates and directions (small arrows) are shown at the trench [*DeMets et al.*, 1990].

fragmenting along this fracture zone. On the basis of our seismic results and these tectonic observations, we propose a slab tear model, wherein the Cocos slab is currently fragmenting into a N Cocos plate and a S Cocos plate along the projection of the OFZ by a pivoting subduction process similar to that which occurred when the Rivera plate separated from the proto-Cocos plate. This ongoing fragmentation event presents the opportunity to observe and study a young tearing process in action.

[26] **Acknowledgments.** This study was supported in part by the Gordon and Betty Moore Foundation through the Tectonics Observatory at California Institute of Technology. This is contribution number 207 from the Caltech Tectonics Observatory. We are grateful to the Incorporated Research Institutions for Seismology Data Management Center (IRIS-DMC) for making the waveform data available. We thank Arturo Iglesias for providing the Servicio Sismológico Nacional event catalog. We also thank Editor Robert Nowack and two anonymous reviewers for helpful comments which greatly improved the manuscript.

References

Allan, J. F. (1986), Geology of the Northern Colima and Zacoalco Grabens, southwest Mexico: Late Cenozoic rifting in the Mexican Volcanic Belt, *Geol. Soc. Am. Bull.*, *97*, 473–485.

Atwater, T. (1989), Plate tectonic history of the northeast Pacific and western North America, in *The Eastern Pacific Ocean and Hawaii*, *Geol. North Am.*, vol. N, edited by E. L. Winterer, D. M. Hussong and R. W. Decker, pp. 21–72, Geol. Soc. Am., Boulder, Colo.

Bandy, W. L., and T. W. C. Hilde (2000), Morphology and recent history of the ridge propagator system located at 18°N, 106°W, in *Cenozoic Tectonics and Volcanism of Mexico*, edited by H. Delgado-Granados, G. Aguirre-Díaz, and J. M. Stock, *Spec. Pap. Geol. Soc. Am.*, *334*, 29–40.

Bandy, W., C. Mortera-Gutierrez, J. Urrutia-Fucugauchi, and T. W. C. Hilde (1995), The subducted Rivera-Cocos plate boundary: Where is it, what is it, and what is its relationship to the Colima rift?, *Geophys. Res. Lett.*, *22*, 3075–3078.

Bandy, W. L., V. Kostoglodov, and C. A. Mortera-Gutiérrez (1998), Southwest migration of the instantaneous Rivera-Pacific euler pole since 0.78 Ma, *Geofis. Int.*, *37*, 153–169.

Bandy, W. L., T. W. C. Hilde, and C.-Y. Yan (2000), The Rivera-Cocos plate boundary: Implications for Rivera-Cocos relative motion and plate fragmentation, in *Cenozoic Tectonics and Volcanism of Mexico*, edited by H. Delgado-Granados, G. Aguirre-Díaz, and J. M. Stock, *Spec. Pap. Geol. Soc. Am.*, *334*, 1–28.

Blatter, D. L., and L. Hammersley (2010), Impact of the Orozco Fracture Zone on the central Mexican Volcanic Belt, *J. Volcanol. Geotherm. Res.*, *197*, 67–84, doi:10.1016/j.volgeores.2009.08.002.

Blatter, D. L., G. L. Farmer, and I. S. E. Carmichael (2007), A North-south transect across the Central Mexican Volcanic Belt at ~100°W: Spatial distribution, petrological, geochemical, and isotopic characteristics of Quaternary volcanism, *J. Petrol.*, *48*, 901–950, doi:10.1093/petrology/egm006.

Bourgois, J., and F. Michaud (1991), Active fragmentation of the North America plate at the Mexican triple junction area off Manzanillo, *Geo Mar. Lett.*, *11*, 59–65.

Bourgois, J., and F. Michaud (2002), Comparison between the Chile and Mexico triple junction areas substantiates slab window development beneath northwestern Mexico during the past 12–10 Myr, *Earth Planet. Sci. Lett.*, *201*, 35–44.

Burbach, G. V., C. Frohlich, W. D. Pennington, and T. Matumoto (1984), Seismicity and tectonics of the subducted Cocos plate, *J. Geophys. Res.*, *89*, 7719–7735.

Burkett, E. R., and M. I. Billen (2010), Three-dimensionality of slab detachment due to ridge-trench collision: Laterally simultaneous boudinage versus tear propagation, *Geochem. Geophys. Geosyst.*, *11*, Q11012, doi:10.1029/2010GC003286.

Chung, W.-Y., and H. Kanamori (1978), Subduction process of a fracture zone and aseismic ridges: The focal mechanism and source characteristics of the New Hebrides earthquake of 1969 January 19 and some related events, *Geophys. J. R. Astron. Soc.*, *54*, 221–240.

Crotwell, H. P., T. J. Owens, and J. Ritsema (1999), The TauP Toolkit: Flexible seismic travel-time and ray-path utilities, *Seismol. Res. Lett.*, *70*, 154–160.

DeMets, C., and S. Traylen (2000), Motion of the Rivera plate since 10 Ma relative to the Pacific and North American plates and the mantle, *Tectonophysics*, *318*, 119–159.

DeMets, C., and D. S. Wilson (1997), Relative motions of the Pacific, Rivera, North American, and Cocos plates since 0.78 Ma, *J. Geophys. Res.*, *102*, 2789–2806.

DeMets, C., R. G. Gordon, D. F. Argus, and S. Stein (1990), Current plate motions, *Geophys. J. Int.*, *101*, 425–478.

Dreger, D. S., and D. V. Helmberger (1993), Determination of source parameters at regional distances with three-component sparse network data, *J. Geophys. Res.*, *98*, 8107–8125.

Eissler, H., and H. Kanamori (1982), A large normal-fault earthquake at the junction of the Tonga trench and the Louisville ridge, *Phys. Earth Planet. Inter.*, *29*, 161–172.

Eissler, H. K., and K. C. McNally (1984), Seismicity and tectonics of the Rivera plate and implications for the 1932 Jalisco, Mexico, earthquake, *J. Geophys. Res.*, *89*, 4520–4530.

Ferrari, L. (2004), Slab detachment control on mafic volcanic pulse and mantle heterogeneity in central Mexico, *Geology*, *32*, 77–80, doi:10.1130/G19887.1.

Ferrari, L., G. Pasquaré, S. Venegas, D. Castillo, and F. Romero (1994), Regional tectonics of western Mexico and its implications for the northern boundary of the Jalisco block, *Geofis. Int.*, *33*, 139–151.

Franco, S. I., V. Kostoglodov, K. M. Larson, V. C. Manea, M. Manea, and J. A. Santiago (2005), Propagation of the 2001–2002 silent earthquake

and interplate coupling in the Oaxaca subduction zone, Mexico, *Earth Planets Space*, *57*, 973–985.

Franke, D., M. Schnabel, S. Ladage, D. R. Tappin, S. Neben, Y. S. Djajadihardja, C. Muller, H. Kopp, and C. Gaedicke (2008), The great Sumatra-Andaman earthquakes: Imaging the boundary between the ruptures of the great 2004 and 2005 earthquakes, *Earth Planet. Sci. Lett.*, *269*, 118–130, doi:10.1016/j.epsl.2008.01.047.

Hall, C. E., and M. Gurnis (2005), Strength of fracture zones from their bathymetric and gravitational evolution, *J. Geophys. Res.*, *110*, B01402, doi:10.1029/2004JB003312.

Huchon, P., and J. Bourgois (1990), Subduction-induced fragmentation of the Nazca Plate off Peru: Mendana Fracture Zone and Trujillo Trough revisited, *J. Geophys. Res.*, *95*, 8419–8436.

Husker, A., and P. M. Davis (2009), Tomography and thermal state of the Cocos plate subduction beneath Mexico City, *J. Geophys. Res.*, *114*, B04306, doi:10.1029/2008JB006039.

Kim, Y., R. W. Clayton, and J. M. Jackson (2010), Geometry and seismic properties of the subducting Cocos plate in central Mexico, *J. Geophys. Res.*, *115*, B06310, doi:10.1029/2009JB006942.

Klitgord, K. D., and J. Mammerickx (1982), Northern East Pacific Rise: Magnetic anomaly and bathymetric framework, *J. Geophys. Res.*, *87*, 6725–6750.

Kostoglodov, V., and L. Ponce (1994), Relationship between subduction and seismicity in the Mexican part of the Middle America trench, *J. Geophys. Res.*, *99*, 729–742.

Lonsdale, P. (1991), Structural patterns of the Pacific floor offshore of peninsular California, in *The Gulf and Peninsular Province of the Californias*, edited by J. P. Dauphin and B. R. T. Simoneit, *AAPG Mem.*, *47*, 87–125.

Lonsdale, P. (2005), Creation of the Cocos and Nazca plates by fission of the Farallon plate, *Tectonophysics*, *404*, 237–264, doi:10.1016/j.tecto.2005.05.011.

Lowrie, A., C. Smoot, and R. Batiza (1986), Are oceanic fracture zones locked and strong or weak?: New evidence for volcanic activity and weakness, *Geology*, *14*, 242–245.

Luhr, J. F., S. A. Nelson, J. F. Allan, and I. S. E. Carmichael (1985), Active rifting in southwestern Mexico: Manifestations of an incipient eastward spreading-ridge jump, *Geology*, *13*, 54–57.

Lynn, W. S., and B. T. R. Lewis (1976), Tectonic evolution of the northern Cocos plate, *Geology*, *4*, 718–722.

Mammerickx, J., and K. D. Klitgord (1982), Northern East Pacific Rise: Evolution from 25 m.y. B.P. to the present, *J. Geophys. Res.*, *87*, 6751–6759.

Manea, V., and M. Gurnis (2007), Subduction zone evolution and low viscosity wedges and channels, *Earth Planet. Sci. Lett.*, *264*, 22–45, doi:10.1016/j.epsl.2007.08.030.

Manea, V. C., M. Manea, V. Kostoglodov, C. A. Currie, and G. Sewell (2004), Thermal structure, coupling and metamorphism in the Mexican subduction zone beneath Guerrero, *Geophys. J. Int.*, *158*, 775–784, doi:10.1111/j.1365-246X.2004.02325.x.

McCann, W. R., and R. E. Habermann (1989), Morphologic and geologic effects of the subduction of bathymetric highs, *Pure Appl. Geophys.*, *129*, 41–69.

Menard, H. W. (1978), Fragmentation of the Farallon Plate by pivoting subduction, *J. Geology*, *86*, 99–110.

Nixon, G. T. (1982), The relationship between Quaternary volcanism in central Mexico and the seismicity and structure of subducted ocean lithosphere, *Geol. Soc. Am. Bull.*, *93*, 514–523.

Noriega-Manzanedo, F., and X. Pérez-Campos (2010), Comparación de catálogos sísmicos públicos para sismos mexicanos, *GEOS, Unión Geofísica Mexicana*, *30*(1), 165.

Pacheco, J. F., and S. K. Singh (2010), Seismicity and state of stress in Guerrero segment of the Mexican subduction zone, *J. Geophys. Res.*, *115*, B01303, doi:10.1029/2009JB006453.

Pardo, M., and G. Suárez (1995), Shape of the subducted Rivera and Cocos plates in southern Mexico: Seismic and tectonic implications, *J. Geophys. Res.*, *100*, 12,357–12,373.

Pérez-Campos, X., Y. Kim, A. Husker, P. M. Davis, R. W. Clayton, A. Iglesias, J. F. Pacheco, S. K. Singh, V. C. Manea, and M. Gurnis (2008), Horizontal subduction and truncation of the Cocos Plate beneath central Mexico, *Geophys. Res. Lett.*, *35*, L18303, doi:10.1029/2008GL035127.

Porritt, R. W., R. M. Allen, D. C. Boyarko, and M. R. Brudzinski (2011), Investigation of Cascadia segmentation with ambient noise tomography, *Earth Planet. Sci. Lett.*, *309*, 67–76, doi:10.1016/j.epsl.2011.06.026.

Ramírez-Herrera, M. T., V. Kostoglodov, and J. Urrutia-Fucugauchi (2011), Overview of recent coastal tectonic deformation in the Mexican subduction zone, *Pure Appl. Geophys.*, *168*, 1415–1433, doi:10.1007/s00024-010-0205-y.

Rosenbaum, G., M. Gasparon, F. P. Lucente, A. Peccerillo, and M. S. Miller (2008), Kinematics of slab tear faults during subduction segmentation and implications for Italian magmatism, *Tectonics*, *27*, TC2008, doi:10.1029/2007TC002143.

Russo, R. M., and P. G. Silver (1994), Trench-parallel flow beneath the Nazca plate from seismic anisotropy, *Science*, *263*, 1105–1111.

Schellart, W. P., J. Freeman, D. R. Stegman, L. Moresi, and D. May (2007), Evolution and diversity of subduction zones controlled by slab width, *Nature*, *446*, 308–311, doi:10.1038/nature05615.

Serrato-Díaz, G. S., W. L. Bandy, and C. A. Mortera-Gutiérrez (2004), Active rifting and crustal thinning along the Rivera-Cocos plate boundary as inferred from mantle bouguer gravity anomalies, *Geofís. Int.*, *43*, 361–381.

Sigloch, K. (2011), Mantle provinces under North America from multifrequency P wave tomography, *Geochem. Geophys. Geosyst.*, *12*, Q02W08, doi:10.1029/2010GC003421.

Sillitoe, R. H. (1974), Tectonic segmentation of the Andes: Implications for magmatism and metallogeny, *Nature*, *250*, 542–545.

Singh, S. K., and M. Pardo (1993), Geometry of the Benioff zone and state of stress in the overriding plate in central Mexico, *Geophys. Res. Lett.*, *20*, 1483–1486.

Song, T. A., D. V. Helmberger, M. R. Brudzinski, R. W. Clayton, P. Davis, X. Pérez-Campos, and S. K. Singh (2009), Subducting slab ultra-slow velocity layer coincident with silent earthquakes in southern Mexico, *Science*, *324*, 502–506.

Soto, G. L., J. F. Ni, S. P. Grand, E. Sandvol, R. W. Valenzuela, M. G. Speziale, J. M. G. González, and T. D. Reyes (2009), Mantle flow in the Rivera-Cocos subduction zone, *Geophys. J. Int.*, *179*, 1004–1012, doi:10.1111/j.1365-246X.2009.04352.x.

Stock, J. M., and J. Lee (1994), Do microplates in subduction zones leave a geological record?, *Tectonics*, *13*, 1472–1487.

Stubailo, I., C. Beghein, and P. M. Davis (2012), Structure and anisotropy of the Mexico subduction zone based on Rayleigh-wave analysis and implications for the geometry of the Trans-Mexican Volcanic Belt, *J. Geophys. Res.*, *117*, B05303, doi:10.1029/2011JB008631.

Vogt, P. R., A. Lowrie, D. R. Bracey, and R. N. Hey (1976), *Subduction of Aseismic Oceanic Ridges: Effects on Shape, Seismicity, and Other Characteristics of Consuming Plate Boundaries*, *Spec. Pap. Geol. Soc. Am.*, *172*, 59 p.

Wortel, R., and S. Cloetingh (1981), On the origin of the Cocos-Nazca spreading center, *Geology*, *9*, 425–430.

Wortel, R., and S. Cloetingh (1983), A mechanism for fragmentation of oceanic plates, in *Studies in Continental Margin Geology*, edited by J. S. Watkins and C. L. Drake, *AAPG Mem.*, *34*, 793–801.

Yang, T., S. P. Grand, D. Wilson, M. Guzman-Speziale, J. M. Gomez-Gonzalez, T. Dominguez-Reyes, and J. Ni (2009), Seismic structure beneath the Rivera subduction zone from finite-frequency seismic tomography, *J. Geophys. Res.*, *114*, B01302, doi:10.1029/2008JB005830.